Recipient:
Ralph Schneider
NA-113.1
Forrestal Building
1000 Independence Ave SW
Washington, DC 20585

DOE ID: #DE-FG52-98DP00206

FINAL REPORT

Turbulence and Interfacial Mixing

Co-Principal Investigators:
James Glimm and Xiaolin Li
University at Stony Brook

Project Period:
November 15, 1997 – December 31, 2004

Recipient Organization:
Research Foundation
University at Stony Brook
Stony Brook, NY 11794-3366

Unexpended Funds: $0.00

Contents

1 Overview

We study mix from analytical and numerical points of view. These investigations are linked. The analytical studies (in addition to laboratory experiments) provide bench marks for the direct simulation of mix. However, direct simulation is too detailed to be useful and to expensive to be practical. We also consider averaged equations. Here the major issue is the validation of the closure assumptions. We appeal to the direct simulation methods for this step.

We have collaborated with several NNSA teams; moreover, Stony Brook alumni (former students, faculty and research collaborators) presently hold staff positions in NNSA laboratories.

2 Research Accomplishments

2.1 Direct Simulation of Mix

Mixing results from the instability of an interface separating distinct fluids. We consider acceleration driven instabilities, with a density discontinuity at a fluid interface. Constant acceleration (*e.g.* gravity) defines the Rayleigh-Taylor (RT) instability [34], while impulsive acceleration (as by a shock wave) yields the Richtmyer-Meshkov (RM) instability. In the self similar case of constant acceleration, the height, $h(t)$ of the mixing zone as a function of time, t satisfies a scaling relation

$$h(t) = \alpha A g t^2 \ ,$$

where g is the (gravitational) acceleration, $A = (\rho_2 - \rho_1)/(\rho_2 + \rho_1)$ is the Atwood number which is a buoyancy renormalization of g, and α is a dimensionless constant which characterizes the mixing rate. The mixing behavior

is described by the growth rates $\alpha = \alpha_b$ for the bubble side of the mixing layer, measuring the penetration of the light fluid into the ambient heavy fluid, and $\alpha = \alpha_s$ for the spike side of the mixing layer, measuring the penetration of the heavy fluid into the ambient light fluid. For incompressible flows, $\alpha_b \approx 0.06 \pm 0.01$ is a universal constant.

The proposers and co-workers have achieved simulations and theory in agreement with experiment, and thus laid a foundation for a predictive science of mixing. Many open questions remain.

Front Tracking prevents numerical diffusion at the interface, which is a dominant aspect of most simulations of interface dominated flows. In [12], we show that for constant simulation error, a tracked simulation requires a factor of 4 to 8 less resolution, *i.e.* 4^3 or 8^3 fewer space time cells in a 2D simulation.

2.1.1 RM Simulation and ICF Modeling.

In collaboration with a team centered at LLNL and U. Michigan, we simulated axisymmetrically perturbed spherical explosions as performed on NOVA laser experiments [35], with excellent agreement with experiments. Continuing this collaboration, we have coupled FronTier to radiation hydro initial laser accelerations performed at LLNL, and thereby determined the effect of preheat on the initial perturbation. We found, for strong laser pulses, that the as machined perturbation is reduced by about a factor of 2 by the motion associated with the preheat. This indicates that the perturbation design has to be engineered to take the preheat into account, or that the main hydro dynamics needs a corrected initial amplitude for simulation of the subsequent instability growth.

We have successfully performed front tracking simulations [24, 23] for

Richtmyer-Meshkov (RM) instabilities in converging spherical geometry. These instabilities are a central hydrodynamics concern in an inertial confinement fusion (ICF) reactor. The influence of the symmetry axis on the instability evolution and late time mixing was investigated [24, 11], with the main conclusions that (1) this North Pole effect was a real consequence of axisymmetrically perturbed flows, *i.e.* it was not due to numerical effects, (2) the effect occurs late in time and, for spherical flow, is pronounced after reshock, and (3) that the effect is not eliminated through use of spherical harmonic perturbations. We have also analyzed the effect of the shock strength in a spherical RM system [14, 11, 10]. We find scaling invariant with respect to shock strength for fluid mixing statistics. The effectiveness of scaling is better for stronger shock strength. Such a scaling law is important since it allows us to obtain the results for all strong shocks by conducting one strong shock experiment or simulation in that family.

2.1.2 Multimode RT Simulation.

Experimental values for the RT mixing coefficient α_b lie in the range $\alpha_b \approx 0.05 - 0.07$ as determined by Read and Youngs, Smeeton and Youngs, and Dimonte *et al.* The theoretical value is $\approx 0.05 - 0.06$ [7]. *FronTier* simulation gives a value at or near the upper end of the experimental interval, while most simulation codes report values of α_b outside of this experimental range, for example $\alpha_b \approx 0.03$.

We have established that numerical mass diffusion, present in many simulations, is the cause of the differences between *FronTier* and the other simulations [15]. Use of a time dependent Atwood number, computed from the densities observed during the evolution of the instability, shows that the Atwood number, buoyancy force and mixing rates are diminished by about 1/2

$\alpha_{\text{experiment}}$	$\approx 0.05 - 0.07$
α_{theory}	$\approx 0.05 - 0.06$ [7]
α_{FronTier}	≈ 0.07
α_{TVD}	≈ 0.04
$\alpha_{\text{TVD,eff}}$	≈ 0.07

Table 1: α_{b} as determined by experiment, theory, and the calculations reported here. The untracked TVD simulation is diffusive, but a renormalized α, using the time dependent Atwood number to compensate for the mass diffusion of the simulation, allows agreement among all values of α reported here.

in untracked simulations but not in tracked simulations, due to numerical mass diffusion. This same numerical mass diffusion is also a possible cause for the disagreement between experiment and many simulations. See Table 1. Physical mass diffusion must be at least the laminar value cited in handbooks, but could be larger if a transition to turbulence has occured. Noise in the initial conditions has also been proposed as contributing to the value of α_{b}, so the comparison of simulation to experiment requires further study.

In work in progress, we find that the improvements to RT simulations resulting from the use of local grid based tracking increase the value of α_b, placing the FronTier simulations in disagreement with experiment. However, it appears that use of the physical values for surface tension (for immiscible fluids) or physical mass diffusion (for miscible fluids) will improve and possibly restore the agreement with experiment, and show that FronTier is able to distinguish secondary aspects of the physics modeling parameters.

2.1.3 Turbulent Combustion

The nuclear burning in a type Ia supernova explosion gives rise to turbulent combustion. We have conducted 2D axisymmetric simulations which show a successful level of burning. We do not use a turbulent model in the simulation, so that the simulation is free from adjustable parameters related to the hydrodynamics. See [36].

2.2 Averaged Mix Model Equations

Closure is the problem of defining the functional form of the averaged nonlinear terms in the flow equations, as these should not be represented as the nonlinear function of the averaged primitive variables. This is the central problem for averaged equations. In our approach to averaged equations, we require expressions for the interface averaged velocity, pressure and work, namely the quantities v^*, p^*, and $(pv)^*$. As a physics postulate, we suppose that v^* does not depend on spatially dimensional quantities other than the v_k. This is in effect the assumption that the mixing layer has no internal length scales, and represents a coarse graining to eliminate special effects of boundary layers, *etc.*

We have developed a closure which replaces phenomenological drag forces with a model for the pressure differences (pressure drag) between the phases. We have solved this model in closed form in the 1D incompressible limit, and in asymptotics for the weakly compressible limit. Using these solutions, we validated a numerical solution of these equations, see [25, 26] and our earlier papers cited there.

We analyzed the compressible formulation of these equations, and derived a closure which conserves energy. The entropy of smooth flow should not be conserved, as the averaging process, as with a mixing process, is not

adiabatic. Rather, the phase entropies of the averaged quanities (expressed through the thermodynamic relations as a function of the conserved average density and energy) should satisfy an inequality expressing entropy loss during averaging. Imposition of this inequality results in an identity relating the edge motions of the two sides of the mixing layer, confirming earlier work of ours in which the same edge coupling was derived from postulates concerning the center of mass motion of the mixing layer. See [29].

We have shown that modeling the pressure difference between the phases will be a difficult matter in the incompressible limit. We established numerically strong EOS effects in RT mixing for very weakly compressible flows [30]. These effects included averaged phase pressure differences (pressure drag) and shape differences (form drag), but the overall perturbation amplitudes were not sensitive to the EOS.

The above model for closure of the averaged equations has been extended, in the incompressible case, to multilayer mixing [8]. The previously studied case of $n = 2$ layers, *i.e.* a single interface was solvable in closed form, and the general case $n \geq 2$ reduces to the previous case for $n = 2$ and also yields many explicit formulas for $n \geq 3$; details for $n = 3$ are presented.

See the recent survey article [6], emphasizing analytic methods for mix.

2.3 Analytical Studies

2.3.1 The Renormalization Group (RNG).

In the RNG approach, integration over small scales is used to define the effective equations on some intermediate length scale. The introduction of new (small) length scales and the change in location of the intermediate length scale is treated differentially, to give the renormalization group equation. A fixed point for this equation is of special interest. In this case, the problem

formulation and equations do not change as the intermediate length scale is varied. The equations and solutions are self similar. Power law exponents and premultiplying coefficients then determine the solution.

2.3.2 Bubble Merger and RNG.

Our RNG study of the Rayleigh-Taylor instability is based on a statistical model for the dynamic evolution of an ensemble of bubbles, regarded as an approximation to the two fluid Euler equations, describing the fluid evolution directly. The bubble model has its own laws of dynamical evolution. Each bubble moves as the sum of two velocities. The first is due to the bubble itself, and is the terminal velocity taken from single bubble studies. It is a function of the bubble width. The second contribution is a velocity associated with the bubble interactions, and is defined in terms of the relative position of the bubble and its neighbor. It is also derived from single bubble studies of the Rayleigh-Taylor problem. At sufficiently large relative heights, a merger process will occur between adjacent bubbles, leading to a new bubble, of width equal to the combined widths of the two which are merging. This model was extended to 3D and solved to yield agreement with experimental values in both the mixing growth rate $\alpha_b \approx 0.05 - 0.06$ and the bubble height to width ratio [7]. We derived and validated against experimental data a new dynamic relation, relating the bubble growth rate, the bubble width and the fluctuations in the bubble height.

2.3.3 Rayleigh-Taylor Perturbation Theory.

In a series of papers [2, 1, 3] we established a higher order model for the asymptotic velocity of a single RT bubble in 2D and 3D. The model admits multiple solutions, and the slowest moving one is then selected as the phys-

ical solution. The model predicts both the Froude number (the asymptotic velocity) and the width of the bubble. Results compared well to numerical simulations.

2.4 Advanced Numerical Methods

Front Tracking is a numerical method in which surfaces of discontinuity are given explicit computational degrees of freedom, supplementing the continuous solution values at regular grid points [33].

We have developed the Front Tracking simulation code *FronTier*, into a robust, parallelized code, tested on multi-physics, and of critical importance for the simulation results reported here. It is now in public release.

Here we emphasize recent developments in the numerical analysis of front tracking: robustness, simplicity, conservation, and convergence order. See the recent survey articles [11, 13, 16].

2.4.1 Local Grid Based Tracking

Two tracking methods, called grid-free [17] and grid-based tracking [21], have been used to describe the three dimensional interface propagation and its topological bifurcation. The former is a pure Lagrangian method in which the interface propagation and redistribution are independent of the underlying Eulerian grid. The detection and resolution of topological bifurcation is fully determined by the interface itself. This method is more accurate in the propagation of the interface position, but it is not robust in resolving the topological bifurcations. The grid-based tracking method is just the opposite. That is, it is robust in resolving the interface topology, but introduces a larger error in interface propagation. Its handling of the interface topology is through the reconstruction of the interface on Eulerian mesh blocks similar

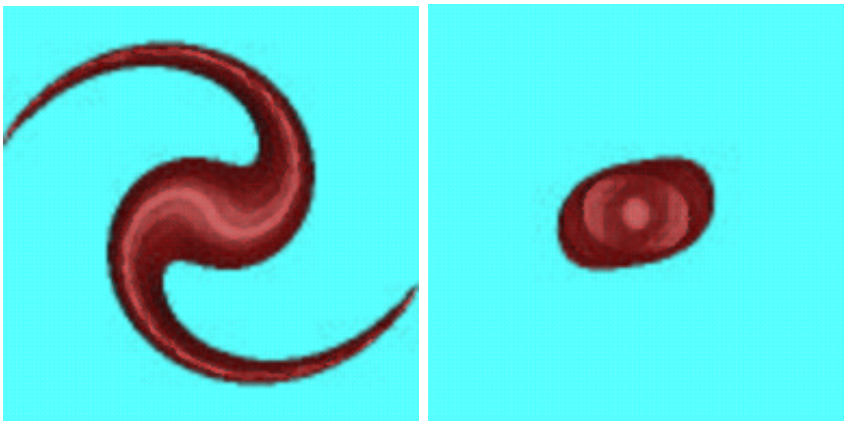

Figure 1: Comparison between Lagrangian propagation and Eulerian reconstructed propagation. In this computation, the initial surface is an ellipsoid. The left plot is the interface after 500 steps of the pure Lagrangian propagation in a spiraling velocity field. The right plot is the Eulerian reconstructed propagation after the same number of steps. The computational mesh is 80^3. The plots show the surfaces after about 1.6 rounds of revolution at the center and 2.86 rounds of revolution at the outer edge (the angular velocity is linear function of r). The loss of accuracy in the right plot (the grid-based simulation) is evident.

to [32]. In Fig. 1, we compare grid-free to grid-based tracking.

We introduce the new locally-grid-based method [9], which combines the advantages of both methods. That is, we use the fully Lagrangian method to propagate the interface to obtain an accurate solution of the interface position. The Eulerian reconstruction of the interface is only used in small regions where a topological bifurcation is detected. Fig. 2 shows the steps of the local reconstruction of the interface.

2.4.2 Conservative Tracking

The solutions to nonlinear hyperbolic systems of conservation laws,

$$u_t + \sum f_i(u)_x = 0 \quad , \tag{1}$$

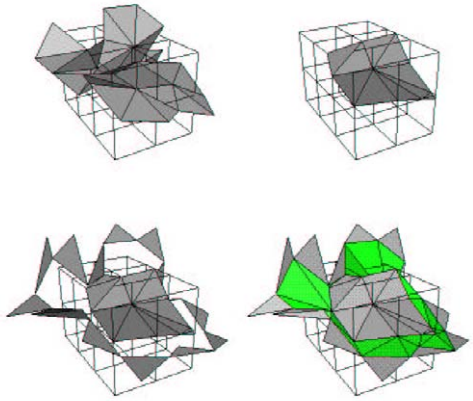

Figure 2: Steps to reconstruct a tangled section of the three dimensional interface. From left to right and top to bottom: (a) assemble blocks which contain unphysical edges, (b) delete triangles attached to the box and rebuild the interface through the grid-based method, (c) reconnect the grid-based interface in the box to its neighbors and (d) the final interface.

develop discontinuities even under smooth initial conditions. The classical front tracking method does not satisfy the conservation property of the system (1). For cells which are cut by the front or cells which miss points of the computational stencil because the stencil crosses the front, the missing points of the stencil are filled in as ghost cells, with the state values obtained by extrapolation from nearby front states of the same component [28].

The proposers and co-workers have introduced a conservative front tracking algorithm. It preserves conservation properties of the system (1) by enforcing conservation for all grid cells, including the ones cut by the front.

The essence of the conservative front tracking algorithm is the tracking of the front in space and time, to construct the space-time finite volume cells, and then solving (1) by

$$|\mathcal{V}_i(t_{n+1})|\bar{u}\ |_{t_{n+1}} = |\mathcal{V}_i(t_n)|\bar{u}\ |_{t_n} - \int_{\partial\mathcal{V}_i} (u, f_i(u)) \cdot n dS\ , \qquad (2)$$

where $\mathcal{V}_i$ is a control volume. This general algorithm works in any dimen-

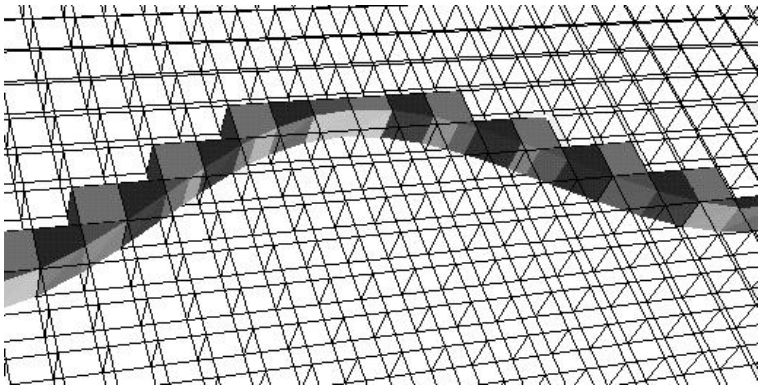

Figure 3: A step in the construction of the conservative algorithm. This step follows the construction of the space time interface and the irregular cells it has cut, and precedes the merger of the small cut cells.

sional space [18].

In [27], the proposers described the 1D and 2D implementation of the conservative tracking algorithm. In 2D conservative tracking, a grid-based spatial interface (the original interface) [22] is first propagated [20, 22, 21, 19]. This yields a general interface, not grid-based, which is then reconstructed to be grid-based [32, 22, 21] (the image interface). The space-time interface is formed by joining these two spatial interfaces (the original and the image interfaces).

We then construct a finite volume decomposition of space time which respects this space-time interface, see Fig. 3. To maintain numerical stability (the CFL time step restriction), we merge those space time cells with small top area to form polyhedra with top area bigger than $0.5\Delta x^2$.

In 2D, the scheme should be second order in the interior region and first order near the front, improving over $\mathcal{O}(1)$ errors commonly found near a discontinuity. The convergence of the bubble growth rate in the simulation of the Richtmyer-Meshkov instability supports this claim. See Figs. 4 and 5.

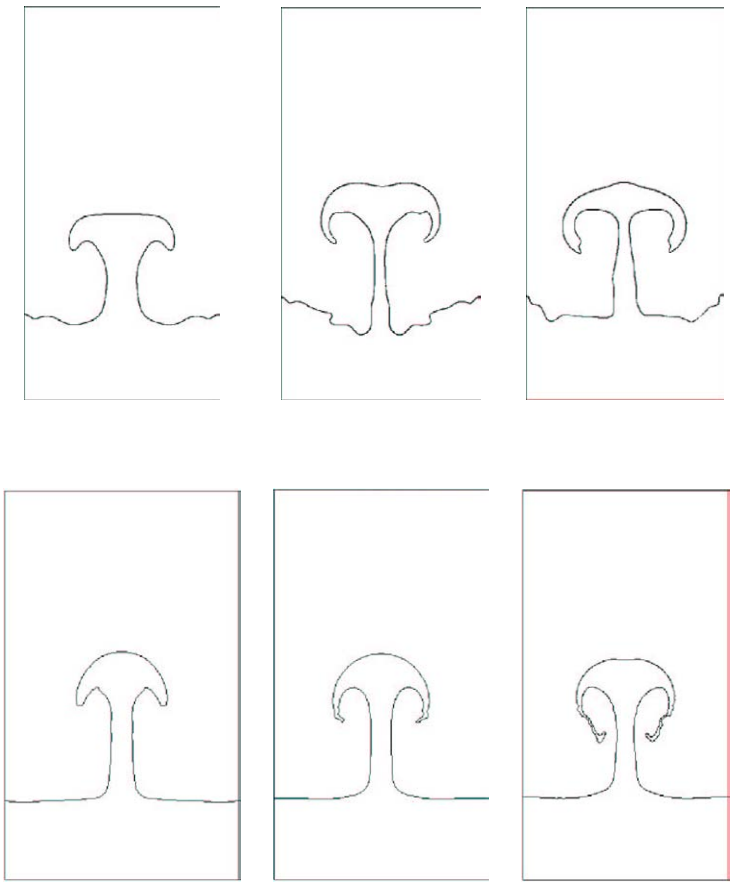

Figure 4: Front plots for RM instability simulations. The upper row shows the plots of a non-conservatively tracked interface at a fixed time. The lower row shows the plots of a conservatively tracked interface at the same time. For both rows, from left to right 40×80, 80×160 and 160×320 grids are used respectively.

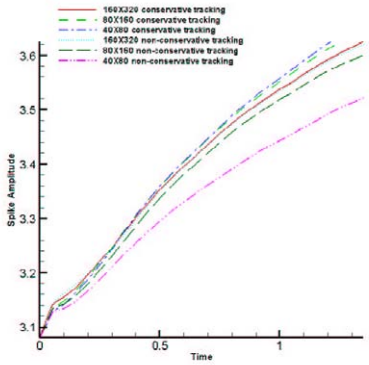

Figure 5: Spike amplitude in the RM instability simulations, as functions of time. The conservative tracked amplitude for a coarse grid is in approximate agreement with the non-conservative tracked amplitude for a fine grid.

2.4.3 Multimaterial Tracking

In general, the grid-based tracking can be extended to an interface separating any number of components. The maximum number of components in a rectangular mesh block is eight. The most useful interface, after the case of two components in a block, is an interface separating three material components in a block. For such an interface in three dimensions, after rotation and commutation, the block interface can be attributed to 57 isomorphically distinct cases. We have built 57 subroutines for the front tracking code to handle all these cases [31]. The tracking of multicomponent interfaces has greatly extended our scope of applications.

2.4.4 Adaptive Mesh Refinement

Adaptive mesh refinement (AMR) is a powerful tool to concentrate computational effort in regions of computational difficulty. Block-structured AMR has been developed systematically by M. Berger and P. Collela [4, 5]. The front

tracking method is also an adaptive method. The authors and co-workers merged the Front Tracking code FronTier with the AMR code Overture, based on the Berger-Colella box refinement algorithm, [4, 5], and developed and maintained at LLNL.

We calculate an axisymmetric spherical RM instability. A Mach 10 imploding spherical shock strikes a spherical contact interface perturbed by 6 modes. We used 3 levels of refinement, with the refinement ratio of 2 and a level 0 grid of 100×100 cells. We compare the result with the comparable uniform grid simulation. The AMR solution matches the uniform fine grid solution as shown by Fig. 6.

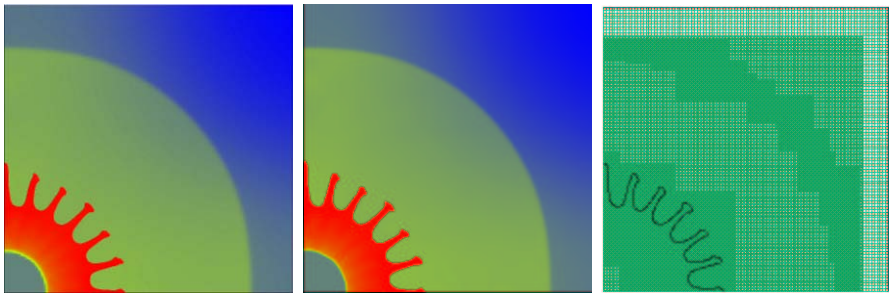

Figure 6: Density and grid plots for the spherical RM simulation at time = 0.3. The left frame shows the density plot from AMR front tracking, and the middle frame shows the density plot from uniform grid front tracking. The right frame shows the AMR grid plots.

3 NNSA Interactions

3.1 NNSA Related Research Collaborations

- David Sharp, John Grove, Baolian Cheng and colleagues at LANL: Studies of mix; uncertainty quantification for mix

- Paul Drake at U. Mich and colleagues at LLNL: Simulation of laser driven mix experiments
- Richard Petrasso and colleagues at MIT: Simulation and modeling of laser driven experiments of mix
- Mark Christon (SNL): numerical methods

3.2 Stony Brook Alumni at NNSA Laboratories

- Former Ph.D. students: Mary Jane Graham Lindquist (LLNL), Cindy Zoldi (LANL) and Richard Holmes (LANL)
- Former Faculty: John Grove (LANL) and Brad Plohr (LANL)
- Former Research Collaborators: John Walter

4 References

[1] S. I. Abarzhi, J. Glimm, and An-Der Lin. Dynamics of the Rayliegh-Taylor bubbles for fluids with a finite density contrast. *Laser and Particle Beams*, 2003. accepted; Stony Brook University Preprint SUNYSB-AMS-02-11.

[2] S. I. Abarzhi, J. Glimm, and An-Der Lin. Rayleigh-Taylor instability for fluids with a finite density contrast. *Phys. Fluids*, 15:2190–2197, 2003.

[3] S. I. Abarzhi, J. Glimm, and K. Nishihara. Rayleigh-Taylor instability and Richtmyer-Meshkov instabilities for fluids with a finite density contrast. *Phys. Lett. A*, 11:1–7, 2003.

[4] M. Berger. Adaptive finite difference methods in fluid dynamics. In *von Karman Lecture Notes on CFD*. 1987. NYU/DOE report 03077-277.

[5] M. Berger and P. Colella. Local adaptive mesh refinement for shock hydrodynamics. *J. Comp. Phys.*, 82:64–84, 1989.

[6] B. Cheng, J. Glimm, H. Jin, and D. H. Sharp. Theoretical methods for the determination of mixing. *Laser and Particle Beams*, 21:429–436, 2003.

[7] B. Cheng, J. Glimm, and D. H. Sharp. A three-dimensional renormalization group bubble merger model for Rayleigh-Taylor mixing. *Chaos*, 12:267–274, 2002.

[8] B. Cheng, J. Glimm, and D. H. Sharp. A multiphase flow model for the unstable mixing of layered materials. *Phys. of Fluids*, 2005. Submitted. LANL Preprint Number LA-UR-05-0078. Stony Brook University Preprint Number SUNYSB-AMS-05-01.

[9] Jian Du, Brian Fix, James Glimm, Hyunsun Lee, Xaiolin Li, and Yunhua Li. A simple package for front tracking. *J. Comp. Phys.*, 2005. Submitted. Stony Brook University preprint SUNYSB-AMS-05-02.

[10] S. Dutta, E. George, J. Glimm, J. Grove, H. Jin, T. Lee, X. Li, D. H. Sharp, K. Ye, Y. Yu, Y. Zhang, and M. Zhao. Shock wave interactions in spherical and perturbed spherical geometries. Elsevier, 2004. In Press; University at Stony Brook preprint number SB-AMS-04-09 and LANL report No. LA-UR-04-2989.

[11] S. Dutta, E. George, J. Glimm, X. L. Li, A. Marchese, Z. L. Xu, Y. M. Zhang, J. W. Grove, and D. H. Sharp. Numerical methods for the

determination of mixing. *Laser and Particle Beams*, 2003. accepted, LANL report No. LA-UR-02-1996.

[12] S. Dutta, J. Glimm, J. W. Grove, D. H. Sharp, and Y. Zhang. Error comparison in tracked and untracked spherical simulations. *Computers and Mathematics with Applications*, 2003. accepted, University at Stony Brook preprint number AMS-03-10 and LANL report No. LA-UR-03-2920.

[13] S. Dutta, J. Glimm, J. W. Grove, D. H. Sharp, and Y. Zhang. A fast algorithm for moving interface problems. In V. Kumar et al., editor, *Computational Science and Its Applications - ICCSA 2003, LNCS 2668*, pages 782–790. Springer-Verlag, Berlin Heidelberg, 2003. LANL report No. LA-UR-02-7895.

[14] S. Dutta, J. Glimm, J. W. Grove, D. H. Sharp, and Y. Zhang. Spherical Richtmyer-Meshkov instability for axisymmetric flow. *Mathematics and Computers in Simulations*, 65:417–430, 2004. University at Stony Brook preprint number AMS-03-13.

[15] E. George and J. Glimm. Self similarity of Rayleigh-Taylor mixing rates. *Phys. Fluids*, 2004. Submitted. Stony Brook University Preprint number SUNYSB-AMS-04-05.

[16] E. George, J. Glimm, J. W. Grove, X. L. Li, Y. J. Liu, Z. L. Xu, and N. Zhao. Simplification, conservation and adaptivity in the front tracking method. In T. Hou and E. Tadmor, editors, *Hyperbolic Problems: Theory, Numerics, Applications*, pages 175–184. Springer Verlag, Berlin and New York, 2003.

[17] J. Glimm, M. J. Graham, J. W. Grove, X.-L. Li, T. M. Smith, D. Tan, F. Tangerman, and Q. Zhang. Front tracking in two and three dimensions. *Comput. Math. Appl.*, 35(7):1–11, 1998.

[18] J. Glimm, J. W. Grove, X. L. Li, Yingjie Liu, and Zhiliang Xu. Unstructured grids in 3D and 4D for time-dependent interface in front tracking with improved accuracy. In B. K. Soni et al., editor, *Proc. 8th Int. Conf. Num. Grid Generation in Comp. Field Simulations*, pages 179–188. 2002. LANL report No. LA-UR-02-0893.

[19] J. Glimm, J. W. Grove, X. L. Li, W. Oh, and D. H. Sharp. A critical analysis of Rayleigh-Taylor growth rates. *J. Comp. Phys.*, 169:652–677, 2001.

[20] J. Glimm, J. W. Grove, X.-L. Li, K.-M. Shyue, Q. Zhang, and Y. Zeng. Three dimensional front tracking. *SIAM J. Sci. Comp.*, 19:703–727, 1998.

[21] J. Glimm, J. W. Grove, X.-L. Li, and D. C. Tan. Robust computational algorithms for dynamic interface tracking in three dimensions. *SIAM J. Sci. Comp.*, 21:2240–2256, 2000.

[22] J. Glimm, J. W. Grove, X.-L. Li, and N. Zhao. Simple front tracking. In G.-Q. Chen and E. DiBenedetto, editors, *Contemporary Mathematics*, volume 238, pages 133–149. Amer. Math. Soc., Providence, RI, 1999.

[23] J. Glimm, J. W. Grove, and Y. Zhang. Three dimensional axisymmetric simulations of fluid instabilities in curved geometry. In M. Rahman and C. A. Brebbia, editors, *Advances in Fluid Mechanics III*, pages 643–652. WIT Press, Southampton, UK, 2000.

[24] J. Glimm, J. W. Grove, Y. Zhang, and S. Dutta. Numerical study of axisymmetric Richtmyer-Meshkov instability and azimuthal effect on spherical mixing. *J. Stat. Physics*, 107:241–260, 2002.

[25] J. Glimm, H. Jin, M. Laforest, F. Tangerman, and Y. Zhang. A two pressure numerical model of two fluid mixing. *SIAM J. Multiscale Model. Simul.*, 1:458–484, 2003.

[26] J. Glimm, H. Jin, and Y. Zhang. Front tracking for multiphase fluid mixing. In A. A. Mammoli and C. A. Brebbia, editors, *Computational Methods in Multiphase Flow II*, pages 13–22. WIT Press, Southampton, UK, 2004.

[27] J. Glimm, X.-L. Li, and Y.-J. Liu. Conservative front tracking with improved accuracy. *SIAM J. Numerical Analysis*, 41:1926–1947, 2003.

[28] J. Glimm, D. Marchesin, and O. McBryan. Subgrid resolution of fluid discontinuities II. *J. Comp. Phys.*, 37:336–354, 1980.

[29] H. Jin, J. Glimm, and D. H. Sharp. Two-pressure two-phase flow models. *ZAMP*, 2003. Submitted. Stony Brook University Preprint number SUNYSB-AMS-03-16 and Los Alamos National Laboratory LAUR Number LA-UR-03-7279.

[30] H. Jin, X. F. Liu, T. Lu, B. Cheng, J. Glimm, and D. H. Sharp. Rayleigh-Taylor mixing rates for compressible flow. *Phys. Fluids*, 2004. In press. Stony Brook University Preprint number SUNYSB-AMS-04-06 and Los Alamos National Laboratory LAUR Number LA-04-1384.

[31] L. Li, J. Glimm, and X.-L. Li. All isomorphic distinct cases for multi-component interfaces in a block. *J. Comp. Appl. Mathematics*, 152:263–276, 2003.

[32] W. E. Lorensen and H. E. Cline. Marching cubes: A high resolution 3D surface construction algorithm. *Computer Graphics*, 21(4):163–169, 1987.

[33] G. Moretti. Computations of flows with shocks. *Ann. Rev. Fluid Mech.*, 19:313–337, 1987.

[34] D. H. Sharp. An overview of Rayleigh-Taylor instability. *Physica D*, 12:3–18, 1984.

[35] Y. Zhang, P. Drake, J. Glimm, J. Grove, and D. H. Sharp. Radiation coupled front tracking simulations for laser driven shock experiments. *J. Nonlinear Analysis*, 2004. Submitted. LANL report No. LA-UR-04-2381.

[36] Y. Zhang, J. Glimm, and S. Dutta. Tracked flame simulation for Type Ia supernova. In *Proceeding of Third MIT Conference*. 2005. Submitted.